

Nonperturbative theory of magnetocrystalline anisotropy energy for wires and rings of Fe adatoms

R. Družinić and W. Hübner*

Institute for Theoretical Physics, Freie Universität Berlin, Arnimallee 14, D-14195 Berlin, Germany

(Received 17 May 1996)

The magnetocrystalline anisotropy energy E_{anis} for free-standing chains (quantum wires) and rings of Fe adatoms $N=(2, \dots, 48)$ is determined using an electronic tight-binding theory. Treating spin-orbit coupling nonperturbatively, we analyze the relationship between the electronic structure of the Fe d electrons and $E_{\text{anis}}(n_d)$, for both the chain and ring conformations. We find that $E_{\text{anis}}(N)$ is larger for wires than for rings or infinite monolayers. Generally $E_{\text{anis}}(n_d)$ decreases in chains upon increasing N , while for rings $E_{\text{anis}}(n_d)$ is essentially independent of N . For increasing N , $E_{\text{anis}}(n_d)$ in rings approaches the results for free-standing monolayers. Small rings exhibit clear odd-even oscillations of $E_{\text{anis}}(N)$. Within our theoretical framework we are able to explain the experimentally observed oscillations of $E_{\text{anis}}(n_d)$ during film growth with a period of one monolayer. Finally, a generalization of Hund's third rule on spin-orbit coupling to itinerant ferromagnets is proposed. [S0163-1829(97)05401-5]

I. INTRODUCTION

Over the past decades information technology has been determined by semiconductor applications. However, recently the technology of such devices has been limited due to the optical wavelength. Thus, quantum structures on the nanoscale can offer interesting perspectives for electronic applications. Manipulations on this scale require us to develop nanotools: Low-temperature scanning tunneling microscopes do not only allow for the *probing* of metallic surfaces with atomic resolution, but also for single-atom *manipulation* on surfaces. It has recently been demonstrated that lateral structures of adatoms can be generated by the scanning tunneling microscope (STM) tip (Crommie and co-workers,^{1,2} Meyer, Zophel, and Rieder,³ Rieder and Baratoff.⁴) Modern STM techniques now allow for the preparation of quantum rings (QR's). Examples of QR's, which have been prepared, are rings of 48 Fe adatoms¹ or stadia.² The latter shape is motivated by the search for quantum-chaotic behavior, which so far has not been successful due to strong scattering of the electrons by the ring atoms. The QR of adsorbate atoms sets boundary condition for the wave function of the substrate surface state. The quantum-mechanical electron distribution of this state can therefore be measured by STM, and is found to be in remarkable agreement with standard predictions of quantum mechanics. However, the magnetic moment and magnetocrystalline anisotropy for these nanoscopic structures have not yet been determined in experiment.

In this paper, we are not interested in the surface state but rather in the magnetic anisotropy properties of the quantum ring itself. Since it is known that the magnetocrystalline anisotropy energy E_{anis} is enhanced in thin magnetic films compared to three-dimensional bulk media, one might speculate about a further increase of E_{anis} upon reduction of the dimensionality to one dimension. Thus we calculate E_{anis} for QR's and quantum wires (QW's). These chains are frequently realized by the enhanced adsorption probability of adatoms on step edges.

We analyze for chains and rings for different numbers N of Fe adatoms how the magnetocrystalline anisotropy energy E_{anis} depends on the electronic structure. To our knowledge, the first attempt of this kind was made by Wang, Wu, and Freeman⁵ for a pair of two Fe atoms to explain the dependence of the electronic states. While they treated spin-orbit coupling (SOC) in second-order perturbation theory, we include SOC completely nonperturbatively without resorting to degenerate or nondegenerate perturbation theory of any order. It is shown that for the diatomic pair there are important contributions to the magnetocrystalline anisotropy energy as a function of the number n_d of d electrons per atom $E_{\text{anis}}(n_d)$ due to the different lifting of band degeneracies for different magnetization directions. We find that $E_{\text{anis}} \propto \lambda_{\text{so}}^2$ is valid for the diatomic pair. However, $E_{\text{anis}}(n_d)$ can change its sign with respect to λ_{so} due to level crossings in the energy-level scheme of the diatomic pair. In the same way we calculate $E_{\text{anis}}(n_d)$ for chains and rings with different numbers N of Fe atoms. In small rings there are oscillations of $E_{\text{anis}}(N)$ between rings with an even or odd number of atoms. For our calculation we use two models: (i) an extension of the diatomic pair model⁵ to N atoms, and (ii) a conventional tight-binding description of the wires and rings including SOC. Our paper is organized as follows: In Sec. II, the diatomic-pair model (Sec. II A) and the tight-binding model (Sec. II B) are presented together with the determination of SOC (Sec. II C) and E_{anis} (Sec. II D). Results for the diatomic-pair model are shown in Sec. III A, while results for the tight-binding model are discussed in Sec. III B.

II. THEORY

A. Diatomic-pair model

We follow the ideas of Wang, Wu, and Freeman, and extend their diatomic pair model to the case of N atoms. We start from the following Hamiltonian:^{6,7}

$$H = \sum_{i,\gamma,\sigma} \epsilon_{i\gamma} c_{i\gamma\sigma}^\dagger c_{i\gamma\sigma} + \sum_{(i,j)\gamma,\beta,\sigma,\sigma'} t_{i\gamma j\beta} c_{i\gamma\sigma}^\dagger c_{j\beta\sigma'} \quad (1)$$

TABLE I. The nonvanishing energy integrals in terms of two-center integrals, which we used for the tight-binding model.

$E_{xy,xy}$	$3l^2m^2(V_{dd\sigma}) + (l^2 + m^2 - 4l^2m^2)(V_{dd\pi}) + (n^2 + l^2m^2)(V_{dd\delta})$
$E_{yz,yz}$	$3m^2n^2(V_{dd\sigma}) + (n^2 + m^2 - 4m^2n^2)(V_{dd\pi}) + (l^2 + m^2n^2)(V_{dd\delta})$
$E_{zx,zx}$	$3n^2l^2(V_{dd\sigma}) + (n^2 + l^2 - 4l^2n^2)(V_{dd\pi}) + (m^2 + l^2n^2)(V_{dd\delta})$
E_{xy,x^2-y^2}	$\frac{3}{2}lm(l^2 - m^2)(V_{dd\sigma}) + 2lm(m^2 - l^2)(V_{dd\pi}) + \frac{1}{2}lm(l^2 - m^2)(V_{dd\delta})$
E_{xy,z^2}	$\sqrt{3}lm[n^2 - \frac{1}{2}(l^2 + m^2)](V_{dd\sigma}) - 2\sqrt{3}lmn^2(V_{dd\pi}) + \frac{1}{2}\sqrt{3}ml(1 + n^2)(V_{dd\delta})$
$E_{x^2-y^2,x^2-y^2}$	$\frac{3}{4}(l^2 - m^2)^2(V_{dd\sigma}) + [l^2 + m^2 - (l^2 - m^2)^2](V_{dd\pi}) + [n^2 + \frac{1}{4}(l^2 - m^2)^2](V_{dd\delta})$
$E_{x^2-y^2,z^2}$	$\frac{1}{2}\sqrt{3}(l^2 - m^2)[n^2 - \frac{1}{2}(l^2 + m^2)](V_{dd\sigma}) + \frac{1}{4}\sqrt{3}(1 + n^2)(l^2 - m^2)(V_{dd\delta})$
E_{z^2,z^2}	$[n^2 - \frac{1}{2}(l^2 + m^2)]^2(V_{dd\sigma}) + 3n^2(l^2 + m^2)(V_{dd\pi}) + \frac{3}{4}(l^2 + m^2)^2(V_{dd\delta})$

The summation is taken over N sites i , while the second sum is over pairs of nearest neighbors. As usual, $c_{i\gamma\sigma}^+$ ($c_{i\gamma\sigma}$) creates (destroys) an electron with spin σ at site i and orbital γ . Furthermore $\epsilon_{i\gamma}$ is the on-site energy of an electron at site i and orbital γ . For simplicity we set $\epsilon_{i\gamma} = 0$, since we consider only orbitals of the $3d$ type. The basis functions ϕ_k , $k = 1, \dots, 5$ ($k = 6, \dots, 10$) are the atomic $3d$ orbitals conventionally denoted by xy , yz , zx , $x^2 - y^2$, and $3z^2 - r^2$, where z denotes the interatomic axis, together with the spin eigenstates $|\uparrow\rangle$ and $|\downarrow\rangle$ with respect to the spin quantization axis z_M . The complete ferromagnetic tight-binding Hamiltonian is

$$H_{\text{tb}} = H + H_{\text{ex}}, \quad (2)$$

with the diagonal on-site matrix $H_{\text{ex}} = \sum H_{\text{ex}}^{(i)}$ and

$$H_{\text{ex}}^{(i)} = \begin{pmatrix} H_{\text{ex}}^{\uparrow\uparrow} & H_{\text{ex}}^{\uparrow\downarrow} \\ H_{\text{ex}}^{\downarrow\uparrow} & H_{\text{ex}}^{\downarrow\downarrow} \end{pmatrix} = \frac{J_{\text{ex}}}{2} \begin{pmatrix} -\mathbf{1} & O \\ O & \mathbf{1} \end{pmatrix}, \quad (3)$$

which is actually independent of i . $\mathbf{1}$ and $-\mathbf{1}$ denote 5×5 diagonal matrices, and O is a 5×5 zero matrix. The matrix of the Hamiltonian H_{tb} is then given by

$$H_{\text{tb}} = \begin{pmatrix} H_{\text{ex}}^{(1)} & H_{\text{inter}}^{(1,2)} & \dots & \dots \\ H_{\text{inter}}^{(2,1)} & H_{\text{ex}}^{(2)} & \dots & \dots \\ \vdots & \vdots & \ddots & H_{\text{inter}}^{(N-1,N)} \\ \vdots & \vdots & H_{\text{inter}}^{(N,N-1)} & H_{\text{ex}}^{(N)} \end{pmatrix}, \quad (4)$$

with the intersite Hamiltonian matrix

$$H_{\text{inter}}^{(i,j)} = \begin{pmatrix} H_{\text{inter}}^{\uparrow\uparrow} & O \\ O & H_{\text{inter}}^{\downarrow\downarrow} \end{pmatrix}, \quad (5)$$

where

$$H_{\text{inter}}^{\downarrow\downarrow} = H_{\text{inter}}^{\uparrow\uparrow} = \begin{pmatrix} V_{dd\delta} & 0 & 0 & 0 & 0 \\ 0 & V_{dd\pi} & 0 & 0 & 0 \\ 0 & 0 & V_{dd\pi} & 0 & 0 \\ 0 & 0 & 0 & V_{dd\delta} & 0 \\ 0 & 0 & 0 & 0 & V_{dd\sigma} \end{pmatrix}. \quad (6)$$

Due to the symmetry of the atomic $3d$ orbitals, the dominant overlaps result from the d -orbitals of the same kind, thus yielding nonvanishing contributions only in the diagonal elements of the off-diagonal Hamiltonian $H_{\text{inter}}^{(i,j)}$. Consequently the nearest-neighbor hopping $t_{i\gamma j\beta}$ of Eq. (1) reduces to $t_{i\gamma j\gamma}$, which is equivalent to the three independent nonvanishing interactions $V_{dd\sigma}$, $V_{dd\pi}$, and $V_{dd\delta}$ in Eq. (6). In rings, with periodic boundary conditions, the interaction between the first and last atoms of the corresponding chain must be additionally included. As in Ref. 5 we use $V_{dd\sigma} = -0.25$ eV, $V_{dd\pi} = 0.18$ eV, $V_{dd\delta} = -0.04$ eV, and $J_{\text{ex}} = 3.0$ eV, and a lattice parameter $a = 5.98$ a.u. which matches the fictitious W(001) substrate.

B. Tight-binding model

The main disadvantage of the diatomic pair model is its unrealistic description of tilted d bonds. To perform more realistic calculations of $E_{\text{anis}}(n_d)$ in rings, we have to consider how the bond angles are changed between nearest neighbors of Fe atoms. This aspect is taken into account in the tight-binding model, within the two-center approximation.⁷ The tight-binding Hamiltonian H_{tb} has the same structure for this model as the matrix in Eq. (4). Only the elements of $H_{\text{inter}}^{(i,j)}$ will change their values and positions, because the bond angles have changed. The Hamiltonian is parametrized in terms of the two-center integrals $E_{d,d}(l, m, n)$ of Slater and Koster,⁷ given in Table I, with d as one of the five $3d$ functions xy , yz , zx , $x^2 - y^2$, and z^2 , the latter denoting $3z^2 - r^2$ for simplicity. The direction of the vector $R_j - R_i$, pointing along the bond from one atom to each of its nearest neighbors, is given by the direction cosines l , m , and n . Thus in the tight-binding model both blocks $H_{\text{inter}}^{\uparrow\uparrow} = H_{\text{inter}}^{\downarrow\downarrow}$ of $H_{\text{inter}}^{(i,j)}$ change to

$$\begin{pmatrix} E_{xy,xy} & 0 & 0 & E_{xy,x^2-y^2} & E_{xy,z^2} \\ 0 & E_{yz,yz} & 0 & 0 & 0 \\ 0 & 0 & E_{zx,zx} & 0 & 0 \\ E_{x^2-y^2,xy} & 0 & 0 & E_{x^2-y^2,x^2-y^2} & E_{x^2-y^2,z^2} \\ E_{z^2,xy} & 0 & 0 & E_{z^2,x^2-y^2} & E_{z^2,z^2} \end{pmatrix}. \quad (7)$$

Since we take the (x, y) plane as the ring or chain plane, all direction cosines n must be zero. This thus further simplifies

the nonvanishing two-center integrals of Table I. The other two direction cosines l and m are determined by the bond angle between the Fe atoms.

If we calculate the magnetic anisotropy of single or double chains we assume them to lie also in the (x, y) plane, and to be parallel to the x axis. We couple them either ferromagnetically or antiferromagnetically, by changing the sign of J_{ex} .

C. Spin-orbit coupling

Magnetocrystalline anisotropy is caused by SOC between the d states. SOC is introduced in the usual spherical on-site form as $H_{\text{SO}} = \lambda_{\text{SO}} \mathbf{l} \cdot \mathbf{s}$, with the orbital and spin-moment vectors \mathbf{l} and \mathbf{s} , respectively, and the atomic spin-orbit coupling constant λ_{SO} . Expressing the components of the orbital momentum operator \mathbf{l} in the rotated frame (x_M, y_M, z_M) , where z_M is the spin quantization axis, which is parallel to the direction of magnetization (θ, ϕ) , we may rewrite $H_{\text{SO}} = \sum H_{\text{SO}}^{(i)}$ in the following form:^{8,9}

$$H_{\text{SO}}^{(i)} =: \begin{pmatrix} H_{\text{SO}}^{\uparrow\uparrow} & H_{\text{SO}}^{\uparrow\downarrow} \\ H_{\text{SO}}^{\downarrow\uparrow} & H_{\text{SO}}^{\downarrow\downarrow} \end{pmatrix} = \frac{\lambda_{\text{SO}}}{2} \begin{pmatrix} l_{z_M} & l_{x_M} - il_{y_M} \\ l_{x_M} + il_{y_M} & -l_{z_M} \end{pmatrix}. \quad (8)$$

Here $H_{\text{SO}}^{\uparrow\uparrow} = -H_{\text{SO}}^{\downarrow\downarrow}$ and $H_{\text{SO}}^{\uparrow\downarrow} = -(H_{\text{SO}}^{\downarrow\uparrow})^*$, with

$$H_{\text{SO}}^{\uparrow\uparrow} = \frac{\lambda_{\text{SO}}}{2} \begin{pmatrix} 0 & iv & -iu & 2iw & 0 \\ -iv & 0 & iw & -iu & -\sqrt{3}iu \\ iu & -iw & 0 & -iv & \sqrt{3}iv \\ -2iw & iu & iv & 0 & 0 \\ 0 & \sqrt{3}iu & -\sqrt{3}iv & 0 & 0 \end{pmatrix} \quad (9)$$

and

$$H_{\text{SO}}^{\downarrow\downarrow} = \frac{\lambda_{\text{SO}}}{2} \begin{pmatrix} 0 & v' & -u' & 2w' & 0 \\ -v' & 0 & w' & -u' & -\sqrt{3}u' \\ u' & -w' & 0 & -v' & \sqrt{3}v' \\ -2w' & u' & v' & 0 & 0 \\ 0 & \sqrt{3}u' & -\sqrt{3}v' & 0 & 0 \end{pmatrix}. \quad (10)$$

The variables $u, v, w, u', v',$ and w' are given by $u = \sin\theta_M \cos\phi_M$, $v = \sin\theta_M \sin\phi_M$, $w = \cos\theta_M$, $u' = -\sin\phi_M + i \cos\theta_M \cos\phi_M$, $v' = \cos\phi_M + i \cos\theta_M \sin\phi_M$, and $w' = -i \sin\theta_M$. The value for the SOC constant λ_{SO} is taken from the Fe atom¹⁰: $\lambda_{\text{SO}} = 50$ meV.

Now we have set up the Hamiltonian matrix in terms of the magnetization direction (θ, ϕ) . Since SOC operates to a good approximation only on site, the matrix elements of H_{SO}^i occur exclusively in the diagonal blocks of H_{tb} in Eq. (4); consequently, the matrix elements really occur only in the diagonal and off-diagonal blocks of $H_{\text{ex}}^{(i)}$. For chains, $H_{\text{SO}}^{(i)}$ is independent of site i , while for rings the situation is more complicated. If the magnetic moments are all parallel,

$H_{\text{SO}}^{(i)}$ is independent of the site index i . However, if the magnetic moments have a radial configuration, $H_{\text{SO}}^{(i)}$ does depend on i .

Now the total Hamiltonian H_{tot} is

$$H_{\text{tot}} = H + H_{\text{ex}} + H_{\text{SO}}.$$

In our treatment SOC is included nonperturbatively.¹¹ So we also obtain contributions to $E_{\text{anis}}(n_d)$ from higher-order perturbation theory and may obtain information about the scaling behavior of $E_{\text{anis}}(n_d)$ with the SOC constant λ_{SO} .

D. Anisotropy energy

In both models we define the magnetic anisotropy energy as the difference of energies for perpendicular magnetization E_{\perp} and parallel magnetization E_{\parallel} :

$$E_{\text{anis}}(n_d) := E_{\perp} - E_{\parallel}. \quad (11)$$

Note that for the diatomic pair-model (as defined in Sec. II A) E_{\perp} (E_{\parallel}) refers to magnetization perpendicular (parallel) to the interatomic bonds. For the tight-binding model (as defined in Sec. II B) E_{\perp} (E_{\parallel}), however, refers to magnetization perpendicular (parallel) to the plane of the QR, which is the (x, y) plane. The QW's in this case are assumed to lie in the x direction. Thus E_{\perp} (E_{\parallel}) refers to $\mathbf{M} \parallel \hat{z}$ ($\mathbf{M} \parallel \hat{x}$).

We define the magnetic anisotropy energy per atom for the diatomic-pair model as

$$E_{\text{anis}}(n_d) := E_{\text{tot}}(\theta = \pi/2; n_d) - E_{\text{tot}}(\theta = 0; n_d). \quad (12)$$

Due to the chosen coordinate system, there is no ϕ dependence of $E_{\text{anis}}(n_d)$ in contrast to the tight-binding model. For the tight-binding model we define $E_{\text{anis}}(n_d)$ as

$$E_{\text{anis}}(n_d) := E_{\text{tot}}(\theta = 0; n_d) - E_{\text{tot}}(\theta = \pi/2, \phi; n_d). \quad (13)$$

The in-plane angle ϕ is chosen such that the resulting $|E_{\text{anis}}|$ is the largest possible. $E_{\text{tot}}(\theta, \phi; n_d)$ is the ground-state energy per atom of the chain or ring with a total of n_d $3d$ electrons per atom, N Fe atoms, and the magnetization direction denoted by (θ, ϕ) .⁹ Using the so-called ‘‘force theorem’’ the total energy per atom E_{tot} is given by

$$E_{\text{tot}}(\theta, \phi; n_d) = \frac{1}{N} \sum_m E_m(\theta, \phi) f_0(E_m(\theta, \phi) - E_F(\theta, \phi; n_d)).$$

Here $f_0(\Delta E)$ is the Fermi function at zero temperature and $E_F(\theta, \phi; n_d)$ is the Fermi energy. For a given bandfilling n_d , $E_F(\theta, \phi; n_d)$ is determined self-consistently by

$$n_d = \frac{1}{N} \sum_m f_0(E_m(\theta, \phi) - E_F(\theta, \phi; n_d)).$$

The m th eigenvalue of the total Hamiltonian H_{tot} with magnetization along (θ, ϕ) is given by E_m . Note that the magnetic-moment direction enters only by SOC and can be adjusted for each atomic site individually.

There has been an extensive and in part controversial discussion in the literature on the application of the force theorem.^{12–15} Part of this controversy was reconciled in our recent paper.¹⁶ However, some questions remain. In the present paper, however, we do not address this question.

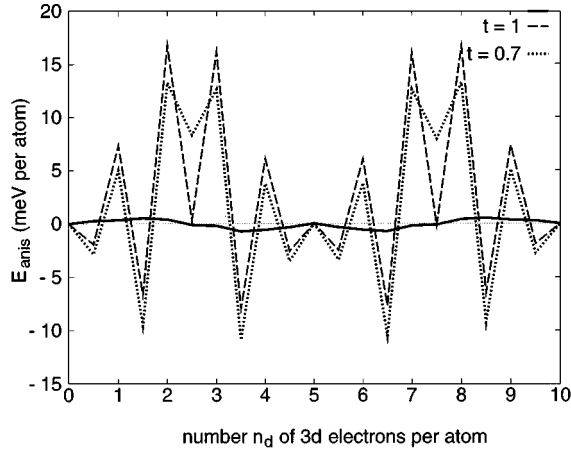


FIG. 1. Dependence of the magnetocrystalline anisotropy energy E_{anis} on the 3d-band filling n_d for a diatomic pair. While the dashed curve refers to the hoppings given in the text, the dotted curve refers to hoppings scaled with an overall factor of $t=0.7$. Negative values of $E_{\text{anis}}(n_d)$ correspond to a perpendicular easy axis. The solid curve shows the contributions of $E_{\text{anis}}^{\text{antipar}}(n_d)$ to $E_{\text{anis}}(n_d)$ from antiparallel spins. As can be seen the main contribution to $E_{\text{anis}}(n_d)$ results from $E_{\text{anis}}^{\text{par}}(n_d)$, due to the large exchange splitting J_{ex} in Fe. The zeros in $E_{\text{anis}}^{\text{antipar}}(n_d)$ at $n_d=2.5$ and 7.5 indicate a sign change imposed by a generalization of Hund's third rule (see text).

Rather we adopt the point of view that the lifting of degeneracies is physically relevant, since it expresses the symmetry of the system. Therefore it should not be omitted, since our calculation mainly focuses on these qualitative symmetry aspects rather than the quantitative values of the magnetocrystalline anisotropy in the chains and rings. Thus a correct nonperturbative treatment of the degeneracies is essential.

Concerning the anticipated magnetic order of the QW and QR in our electronic theory, we make the following remarks: (i) The interatomic distance in our model is chosen in accordance with the lateral lattice constant of a thin bcc-Fe film on a W(001) substrate, which is magnetically ordered. However, the STM experiments produce QR with the interatomic distance of 8–10 Å, which probably would not order, except for possible indirect-exchange effects related to the substrate. Our interest, however, is mainly in small QR's, which might be produced in the near future, with closer nearest-neighbor distances and magnetic order. Furthermore it is important to note that the assumption of magnetic long-range order in our electronic theory is not in contrast to the well-known general theorems of the (ii) Ising¹⁷ and (iii) Heisenberg models.¹⁸

III. RESULTS AND DISCUSSION

A. Results from the diatomic-pair model

In Fig. 1, the magnetocrystalline anisotropy energy $E_{\text{anis}}(n_d)$ per atom is shown as a function of 3d band filling n_d for the Fe diatomic pair (dashed curve). First we note that, as expected, E_{anis} is enhanced compared to Fe monolayers ($E_{\text{anis}}=1, \dots, 16$ meV for the dimer vs ≈ 300 μeV for an Fe monolayer), because of the symmetry reduction from two dimensional (2D) to 1D. This is in accordance with recent studies of magnetism in nickel clusters. Apse, Deng, and

Bloomfield¹⁹ observed enhanced magnetic moments for small nickel clusters and find magnetization minima for clusters with closed geometrical shells and maxima for relatively open clusters.

In Fig. 1, the dependence of $E_{\text{anis}}(n_d)$ on the scaling of all d -electron hopping parameters with an overall parameter t for the diatomic pair is also presented (dotted curve). The absolute value of the magnetic anisotropy energy $|E_{\text{anis}}(n_d)|$ increases for decreasing t (decreasing bandwidth) for the easy axis perpendicular to the bond [$E_{\text{anis}}(n_d) < 0$], and decreases for the easy axis parallel to the bond [$E_{\text{anis}}(n_d) > 0$]. Note that, contrary to the situation in thin films, no convergence problems occur in E_{anis} due to our finite system. Our calculation is performed in real space, and we sum over discrete energy levels. Thus the change of the occupation number is $\Delta n_d = 0.5$, and we obtain 20 points for $E_{\text{anis}}(n_d)$ of the diatomic pair. When the band is completely empty or filled, no contribution to E_{anis} results: $E_{\text{anis}}(n_d=0;10)=0$. While this is trivially the case for an empty band, this relation holds with 14 significant digits for the completely filled case, which yields an independent check of our numerical accuracy. We find for Fe, with its atomic band filling $n_d=6$, an in-plane easy axis for $E_{\text{anis}}(\text{Fe})=6.1$ meV. Since the diatomic pair is a small system, it is not necessary to implicitly assume hybridization with s electrons.

We find for the diatomic pair a mirror symmetry of $E_{\text{anis}}(n_d)$ with respect to half-filling ($n_d=5$), where the spin-up subband is completely full. However, the corresponding points of the curve are not totally symmetric, and a close inspection shows that there are deviations of this mirror symmetry of the order 10^{-5} eV. This small symmetry violation results from the combined action of SOC and the hopping interaction. A detailed analysis shows that this asymmetry increases monotonously with increasing SOC. Especially for $n_d=2.5$ and 7.5 this asymmetry is clearly visible in Fig. 1. To illustrate the origin of this asymmetry we split the spin-orbit coupling matrix H_{SO} into two parts $H_{\text{SO}}^{\text{par}}$ and $H_{\text{SO}}^{\text{antipar}}$ for the coupling between parallel and antiparallel spin states, and recalculate $E_{\text{anis}}(n_d)$ with either of the two matrices instead of H_{SO} itself:

$$H_{\text{SO}} = \begin{pmatrix} H_{\text{SO}}^{\uparrow\uparrow} & 0 \\ 0 & H_{\text{SO}}^{\downarrow\downarrow} \end{pmatrix} + \begin{pmatrix} 0 & H_{\text{SO}}^{\uparrow\downarrow} \\ H_{\text{SO}}^{\downarrow\uparrow} & 0 \end{pmatrix} =: H_{\text{SO}}^{\text{par}} + H_{\text{SO}}^{\text{antipar}}.$$

So we obtain the curve $E_{\text{anis}}^{\text{antipar}}(n_d)$ (solid curve) of Fig. 1, which exhibits a mirror symmetry with respect to half-filling ($n_d=5$). Due to the large exchange splitting J_{ex} , which completely separates the spin subbands, $E_{\text{anis}}^{\text{antipar}}(n_d)$ is very small and thus $E_{\text{anis}} \approx E_{\text{anis}}^{\text{par}}(n_d)$. The $E_{\text{anis}}^{\text{antipar}}(n_d)$ contribution prefers an easy magnetic direction perpendicular (parallel) to the molecule axis if the spin-down subband is less (more) than half-filled, and vice versa for the majority subband, in agreement with the result of Wang, Wu, and Freeman.⁵ Also for larger chains $E_{\text{anis}}^{\text{antipar}}(n_d)$ changes its sign at $n_d=2.5$ and 7.5 , which also seems to be a general trend in Fe monolayers.¹⁶ This is a generalization of Hund's third rule on SOC which applies to itinerant magnetic systems (see the Appendix).

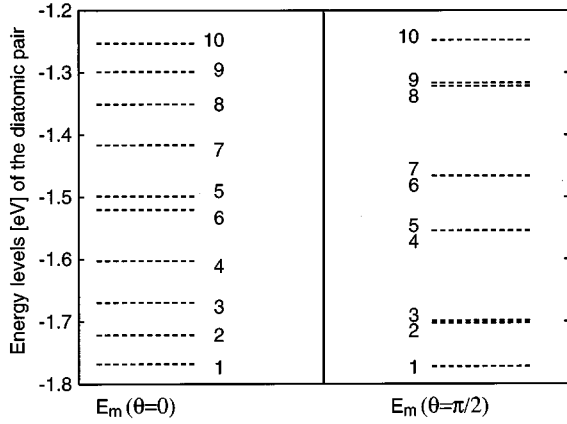


FIG. 2. Energy levels of the diatomic pair for the two magnetization directions $E_m(\theta=0)$ (magnetization in bond direction) and $E_m(\theta=\pi/2)$ (perpendicular to the bond axis). For simplicity only the spin-up states of the energy scale are shown in the plot. For magnetization perpendicular to the bond axis the degeneracies are very weakly lifted by SOC, in contrast to the case of magnetization in the bond direction, where SOC lifts the degeneracies so strongly that levels 5 and 6 intersect.

While for Fe parameters the relation $E_{\text{anis}}^{\text{par}}(n_d) + E_{\text{anis}}^{\text{antipar}}(n_d) \approx E_{\text{anis}}(n_d)$ holds to a good approximation, small deviations are responsible for the asymmetry mentioned above. This asymmetry only occurs if we take into account at least the matrix elements of H_{SO} for the π and δ bonds, and is absent for all other combinations.

The electronic origin of $E_{\text{anis}}(n_d)$ of the diatomic pair can be explained from its energy-level scheme in Fig. 2, for the two magnetization directions $E_m(\theta=0)$ (parallel to molecule axis) and $E_m(\theta=\pi/2)$ (perpendicular to molecule axis). Only the spin-up states are shown in Fig. 2 for simplicity; due to the exchange splitting $J_{\text{ex}}=3.0$ eV, the spin-down states (not shown in the figure) are located symmetrically to these bands with respect to the zero of the energy scale. The individual levels of the spin-up subband have been labeled by the numbers 1, ..., 10 in the absence of SOC. Without SOC, the lowest bonding (level 1) and the highest antibonding states (level 10) result from the splittings caused by $V_{dd\sigma}$. Due to the inequalities $|V_{dd\sigma}| > |V_{dd\pi}| > |V_{dd\delta}|$ (Sec. II B) the lowest bonding and antibonding states are split by $2|V_{dd\sigma}|$, while in each case two doubly degenerate π - (δ -) bonding and antibonding states result from $V_{dd\pi}$ and $V_{dd\delta}$ [see Eq. (6)]. Thus levels 2 and 3 (4 and 5) of Fig. 2 correspond to the π - (δ -) bonding states, while levels 8 and 9 (6 and 7) are equivalent to the corresponding antibonding states. These remaining degeneracies are lifted very strongly by SOC for $E_m(\theta=0)$, and therefore level crossings may occur. For $E_m(\theta=\pi/2)$ the degeneracies are only weakly lifted. The electronic origin of $E_{\text{anis}}(n_d)$ for the diatomic pair results from (i) different SOC-induced *shifting of occupied, nondegenerate levels* for the two magnetization directions, and (ii) *different lifting of degenerate levels*. Note that the lifting of degeneracies can favor a magnetization parallel as well as perpendicular to the bond axis.

Next we investigate the dependence of E_{anis} on λ_{SO} . We find a parabolic shape of $E_{\text{anis}}(\lambda_{\text{SO}})$ for all of the n_d values of the diatomic pair in agreement with Wang, Wu, and

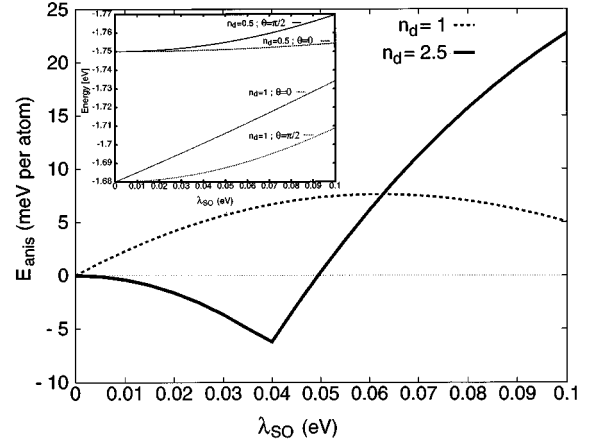


FIG. 3. The dependence of the magnetocrystalline anisotropy energy E_{anis} on λ_{SO} (eV) for $n_d=2.5$ (solid line) and 1 (dashed line) for the diatomic pair. For $n_d=2.5$ a discontinuous change of the slope occurs due to the crossing of levels 5 and 6 in the case of a magnetization parallel to the bond axis. For $n_d=1$ E_{anis} decreases with increasing λ_{SO} . This behavior is explained in the inset of Fig. 3 (see text). The inset shows the shift of levels 1 ($n_d=0.5$) and 2 ($n_d=1$) as a function of λ_{SO} for the diatomic pair and magnetization in bond direction ($\theta=0$) and perpendicular to bond ($\theta=\pi/2$).

Freeman,⁵ irrespective of the value of the spin-orbit coupling constant. To demonstrate this, we show in Fig. 3 the magnetocrystalline anisotropy energy $E_{\text{anis}}(\lambda_{\text{SO}})$ for the band fillings $n_d=1$ and 2.5. In Fig. 3, however, we see a discontinuous change of the slope for $n_d=2.5$, because a level crossing (see Fig. 2) has occurred between levels 5 and 6 for $\lambda_{\text{SO}}=0.04$ eV. The inversion of these levels is indicated by the labeling in Fig. 2, for $\lambda=0.05$ eV. Thus $E_{\text{anis}}(n_d)$ can change its sign because of the level crossings. To explain for $n_d=1$ the dependence of E_{anis} on SOC, we have to study the contribution of level shifts for different magnetization directions. We find that the shifting of *nondegenerate states* is for both magnetization directions proportional to λ_{SO}^2 . For the case of a perpendicular easy axis, the prefactor is larger. The shifting of *degenerate states* for magnetization parallel to the bond axis is in all cases proportional to λ_{SO} , and for magnetization perpendicular to the bond axis proportional to λ_{SO}^2 . To illustrate this, in the inset of Fig. 3 we show the dependence of the level shifts on λ_{SO} for the nondegenerate level 1 (this corresponds to $n_d=0.5$) and the degenerate level 2 ($n_d=1$), for both magnetization directions ($\theta=0; \pi/2$) for the diatomic pair. For $\theta=\pi/2$ and small SOC there is a flat slope of the energy of both levels, while the slope increases with increasing λ_{SO} . Otherwise, the slope of the energy of both levels for $\theta=0$ increases less strongly with increasing λ_{SO} . Thus in Fig. 3 the magnetic anisotropy energy $E_{\text{anis}}(n_d=1)$ decreases for larger SOC with increasing λ_{SO} , as a result of the different position of the energy levels for the two magnetization directions entering the calculation of $E_{\text{anis}}(n_d)$. This yields another reason for the sign change of $E_{\text{anis}}(n_d)$.

Again we point out here that the anisotropy energy exhibits a parabolic shape as a function of spin-orbit coupling (as shown in Fig. 3), although there exist discontinuous derivatives where levels cross. Thus the parabolic shape dominates

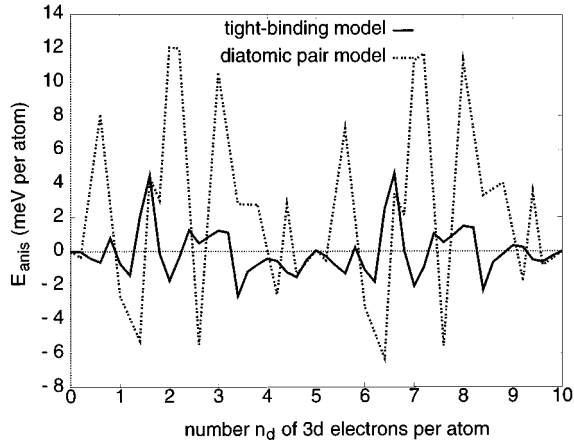


FIG. 4. The dependence of the magnetocrystalline anisotropy energy E_{anis} on the $3d$ -band filling n_d for the five-atom ring calculated in the diatomic pair model (dashed curve) and the tight-binding model (solid curve). In both models, there is a translational symmetry with respect to half-filling $n_d=5$. In the tight-binding model all moments in-plane are chosen to be parallel to each other for this case.

the curve rather than the linear dependence. This is in agreement with the results for free-standing monolayers.^{13,16}

Another important consequence of the level crossing can be seen in Fig. 1. The magnetic anisotropy energy $E_{\text{anis}}(n_d)$ of the quarter-band filling ($n_d=2.5$ and 7.5) of both subbands depends sensitively on the hopping parameters, because the level crossings then occur for smaller values of λ_{SO} (decreasing t), or, in the other case of increasing t for larger values of λ_{SO} .

In Fig. 4 (dashed curve), $E_{\text{anis}}(n_d)$ is shown as a function of $3d$ -band filling n_d for the five-atom Fe ring. In the five-atom ring we find a translational symmetry of $E_{\text{anis}}(n_d)$ with respect to half-filling. This symmetry behavior of $E_{\text{anis}}(n_d)$ is found in all rings with a small odd number $N=(3,7,9,11, \dots)$ of adatoms. In rings, with an even number of atoms and all chains irrespective on whether N is odd or even, we find a mirror symmetry of $E_{\text{anis}}(n_d)$ with respect to half-filling. This behavior is also valid in the tight-binding model, and will be discussed again in Sec. III B. If the number of atoms continues increasing ($N=45,47, \dots$), we then also find a mirror symmetry of $E_{\text{anis}}(n_d)$ with respect to half-filling in odd rings.

B. Results of the tight-binding model

The tight-binding model is better than the diatomic-pair model, because it additionally allows to take into account the following points: (i) The change of the binding angles between nearest neighbors of adatoms in rings is considered in a realistic way. (ii) Due to the extra ϕ dependence of $E_{\text{anis}}(n_d)$ in the tight-binding model, it is possible to choose any magnetic-moment direction in the plane of the ring or chain. (iii) Furthermore, in the tight-binding model it is possible to couple the free-standing chains and rings to the substrate. This extension of the theory, however, has not been performed in this work.

For all chains it is easily checked that $E_{\text{anis}}(n_d)$ is equal in both models. There is a general trend that $E_{\text{anis}}(N)$ decreases

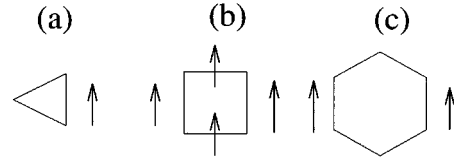


FIG. 5. Odd-even oscillations of the rings (schematic).

with increasing number N of Fe atoms in chains (compare Figs. 1 and 8). For rings this is not the case, as will be discussed below.

The solid curve in Fig. 4 shows $E_{\text{anis}}(n_d)$ for the tight-binding five ring. Although this curve is different from the result in the diatomic-pair model, the translational symmetry survives. A detailed analysis yields that the tight-binding model has the same symmetry behavior for small odd rings as the diatomic-pair model. The translational symmetry can be traced back to the absence of a mirror symmetry between the levels in each of the two spin subbands with respect to $\pm J_{\text{ex}}/2$.

A very important point for the theory of small particles is the existence of a shell structure. Here we discuss in particular the oscillations of E_{anis} as a function of band filling n_d for rings with an even or odd number of adatoms. If the magnetic moment is along the layer normal, it lies in planes perpendicular to all bonds of the ring. But if the magnetic moment lies in the ring plane (assuming exchange-enforced parallel moment alignment), it is *twice* parallel to a bond axis in rings with an even number of N , and *once* in rings with an odd number of N . This is schematically illustrated in Fig. 5 for the trimer [Fig. 5(a)], tetramer [Fig. 5(b)], and hexamer ring [Fig. 5(c)]. In even rings, where N is a multiple of 4 the moment lies also twice perpendicular to a bond axis [see Fig. 5(b)].

We investigate exemplarily, for the four-Fe-atom ring, three different configurations of the magnetic moment direction, which are shown in Fig. 6. Since in larger rings the exchange interaction could possibly not enforce parallel alignment of all magnetic moments, as assumed previously,^{20,21} we calculated $E_{\text{anis}}(n_d)$ for parallel magnetic moment alignment (p), radial moment configurations along the bonds (i), or half of the nearest-neighbor bond angle (h). Since there is a ϕ dependence of $E_{\text{anis}}(n_d)$ in the tight-binding model, we find the following in-plane symmetry in rings for the first two configurations (p) and (i):

$$E_{\text{anis}}(\theta; \phi=0; n_d) = E_{\text{anis}}(\theta; \phi=360/N; n_d). \quad (14)$$

Note that this symmetry is absent for case (h). In Fig. 6, $E_{\text{anis}}(n_d)$ is shown as a function of $3d$ -band filling n_d of the four-atom Fe ring, for the three configurations (p), (i), and (h). Especially for the π bond, the magnetic anisotropy energy $E_{\text{anis}}(n_d)$ has the lowest values for configuration (p). However, this is not the ground-state configuration for Fe with atomic band filling $n_d=6$. For all three configurations we obtain a parallel easy axis of $E_{\text{anis}}(\text{Fe})$, while its value is the largest where the magnetic moments are arranged in configuration (h). This is the ground state of the three configurations for Fe, with the lowest total energy. In order to determine the ground-state configuration for the case of band

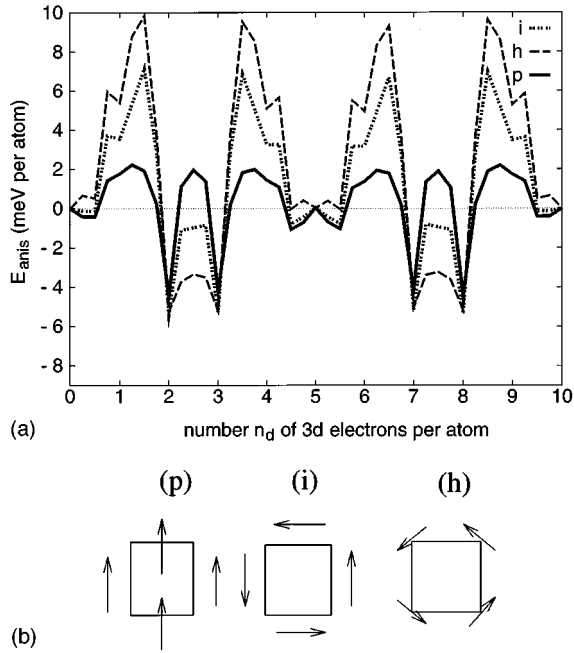


FIG. 6. Dependence of the magnetocrystalline anisotropy energy E_{anis} on the 3d-band filling n_d for a four-atom ring calculated in the tight-binding model for the three displayed magnetic moment configurations. In (p) all moments are parallel to each other, while in (i) and (h) the two radial configurations are given, where all moments are in the bond directions or half to these.

filling around $n_d=7.5$, we have to note that we obtain a perpendicular easy axis for the two radial configurations and an in-plane easy axis for configuration (p). In this case both radial configurations have the same total energy, which has to be compared with the total energy that results from the magnetization in plane (p). A close inspection of all discrete band fillings between $n_d=7$ and 8 shows that configuration (p) has the lowest total energy in this range.

Within our theoretical framework we are able to explain in a simple way a recently discovered phenomenon, viz. oscillations of $E_{\text{anis}}(n_d)$ during film growth with a period of one monolayer.²² The in-plane lattice spacing during epitaxial growth of Co on a Cu(001) single-crystal substrate is found to oscillate as a function of coverage and produces anisotropy oscillations.²³ These oscillations are schematically illustrated in Fig. 7, which shows the connection between the change of the lattice spacing from R to R_1 due to the growth and the corresponding change of E_{anis} . After starting the deposition, Co islands nucleate on the Cu surface. The Co atoms are relaxing in the direction of the center of the island. This gives rise to a reduced in-plane lattice spacing. If the growth of the $N+1$ layer is completed, E_{anis} ($N+1$ layer) nearly returns to the value of E_{anis} (N layer). For uncompleted layers, however, the in-plane lattice constant is very different from that of complete layers and therefore oscillations occur in E_{anis} (N layer) as expected. As a model assumption of this situation the four-atom Fe ring can be considered. We scale all d -electron hopping parameters belonging to one bond of the four-atom Fe ring with a parameter t' , while leaving the others unchanged. Then we also find anisotropy oscillations, due to the changed position of

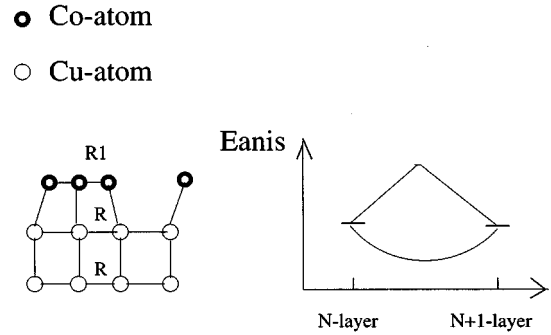


FIG. 7. Schematic sketch of anisotropy oscillations during the growth of Co on Cu. We expect that the change of the lattice spacing from R to R_1 due to the growth of the $(N+1)$ layer will produce oscillations of E_{anis} , which are found in the calculation for the four-atom Fe ring, used to simulate this system.

some levels in the energy-level scheme of the four-atom Fe ring. For decreasing t' for one bond, $E_{\text{anis}}(n_d)$ is increasing or decreasing dependent on n_d . To make our point clear, we again emphasize that there is no oscillatory behavior of the anisotropy with the lattice constant which makes the anisotropy oscillate upon growth but rather an oscillation of the lattice constant itself due to the incompleteness of the growing layer. The anisotropy energy is a smooth function of the lattice constant (also in our calculation), but follows the lattice-constant oscillation.

Finally, in this paper we would like to discuss some results for larger QR's and QW's, in order to reach the experimental situation. In Fig. 8, $E_{\text{anis}}(n_d)$ is shown as a function of 3d-band filling n_d of the 48-atom Fe ring (solid curve), for the p configuration of Fig. 6. A comparison of the three configurations (p, i, and h) shows only marginal deviations of the total energy for the 48 QR's; thus we may assume the p configuration to be the ground state. For an effective band filling of $n_d^{\text{eff}}=6.6$ we find an in-plane easy axis with $E_{\text{anis}}(\text{Fe})=1.45$ meV, assuming implicitly a hybridization of the d electrons with s electrons for this larger system. The shape of the curve is very similar to that of the tight-binding calculations for free-standing Fe monolayers.^{16,24} As can be seen from the comparison of Figs. 8, 4, and 6, $E_{\text{anis}}(N)$ is essentially independent of N .

Since metal atoms aggregating during film growth preferably on step edges [see Ref. 20 for Fe/W(110)] may cause one-dimensional metallization and magnetic properties, it is of interest to calculate the magnetocrystalline anisotropy of larger QW's. The origin of magnetic step anisotropies results from the modified local symmetry of step atoms compared to surface atoms. In Fig. 8, $E_{\text{anis}}(n_d)$ is shown as a function of 3d-band filling n_d for the 48-atom Fe chain, for two different scalings of the hopping parameters (the dashed curve refers to the unscaled case $t=1$). The value of $E_{\text{anis}}(n_d)$ is considerably lower compared to the diatomic pair. However, it is still much larger than the values for free standing Fe monolayers. The shape of the curve for $t=1$ is very similar to the diatomic pair (see Fig. 1), irrespective of the atomic number N . Thus we expect very large contributions to $E_{\text{anis}}(n_d)$ in all chains from SOC-induced lifting of degeneracies. Comparison of Figs. 1 and 8 indicates that, upon decreasing t , the

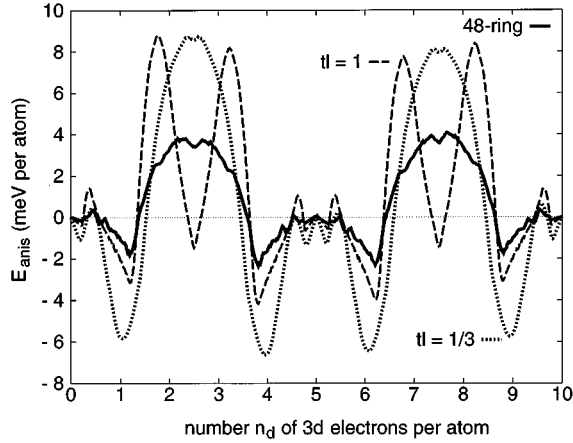


FIG. 8. Dependence of the magnetocrystalline anisotropy energy E_{anis} on the 3d-band filling n_d for a 48-atom ring (solid curve) for the tight-binding model, with the configuration that all moments in plane are parallel to each other. The dashed (dotted) curves shows the dependence of $E_{\text{anis}}(n_d)$ for a 48-atom chain for two different scalings of the hopping $t=1$ ($t=\frac{1}{3}$).

shape of the curve will change similarly for the 48-atom QW, and for the dimer due to level crossings.

In order to show how sensitive the magnetocrystalline anisotropy energy depends on spin configuration, we calculate $E_{\text{anis}}(n_d)$ for two 48-atom Fe chains which are antiferromagnetically (AF) or ferromagnetically (FM) coupled to each other (Fig. 9). In these 96-atom systems $E_{\text{anis}}(N)$ has further decreased in both cases. In AF coupled chains $E_{\text{anis}}(n_d)$ is less dependent on the scaling of the interchain hopping than in FM coupled chains. Note that the shape of $E_{\text{anis}}(n_d)$ for AF coupled chains is similar to that of the 48-atom Fe chain. In this case the shape will not change if the interchain hopping tl is varied, in contrast to FM coupled chains. Thus the breakdown of the one dimensionality in two FM coupled chains will change $E_{\text{anis}}(n_d)$ very strongly. We find in this case a perpendicular easy axis with $E_{\text{anis}}(\text{Fe}) = -0.36$ meV ($tl = 1$). This value is of the same order of magnitude as for Fe monolayers. Experimental results show²⁵ that surface and step anisotropies are of the same order of magnitude, both exhibiting symmetry-breaking as was introduced by Néel's phenomenological model.^{26,27} This is in agreement with our results for two FM coupled chains. The opposite sign and same order of magnitude for surface and step anisotropies is reproduced.

ACKNOWLEDGMENT

We would like to thank Professor K. H. Bennemann for many stimulating discussions and his continued support of this work.

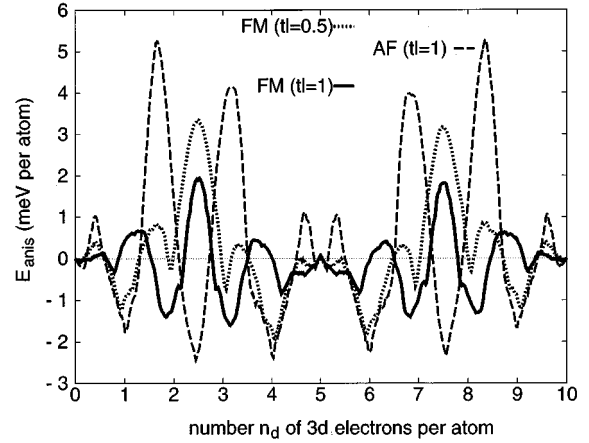


FIG. 9. Dependence of the magnetocrystalline anisotropy energy E_{anis} on the 3d-band filling n_d for two antiferromagnetically (dashed curve) and ferromagnetically (solid and dotted curve) coupled 48-atom Fe chains for the tight-binding model.

APPENDIX: HUND'S THIRD RULE

The curve of $E_{\text{anis}}^{\text{antipar}}(n_d)$ changes its sign at $n_d=2.5$ and 7.5 (see Fig. 1). This sign change occurs exactly, when in each case the two subbands are half filled.

Wang, Wu, and Freeman⁵ also found this behavior for SOC between the opposite spin states for the dimer which can be understood from the following equation (z denoting the symmetry axis and x an arbitrary direction in the perpendicular plane):

$$\Delta E_{\text{ud}} = E_{\text{ud}}(x) - E_{\text{ud}}(z) = \frac{\xi^2}{\Delta E_{\text{ex}}} \sum_{o^-} \langle o^- | \frac{1}{2}(3L_z^2 - L^2) | o^- \rangle. \quad (\text{A1})$$

$ud(o^-)$ represents SOC between the opposite spin states (represents occupied spin-down states), and ΔE_{ex} is the exchange splitting. The sign of ΔE_{ud} depends only on the axial component of the angular momentum. Three states ($L_z = 0, \pm 1$), which are first occupied, make negative contributions, and two ($L_z = \pm 2$) contribute positively. Due to the hybridization, the two antibonding states with $L_z = \pm 2$, which contribute positively, will be occupied next, and therefore it comes to a sign change.

This behavior is also valid in larger chains and monolayers.^{16,24} If one spin subband is half-filled, there is $L=0$, and from this results no contribution to the anisotropy energy. The antibonding states will be occupied in reverse order, and thus there is a sign change at $n_d=2.5$ and 7.5 .

*Corresponding author.

¹M. F. Crommie, C. P. Lutz, and D. M. Eigler, *Science* **262**, 218 (1993).

²E. J. Heller, M. F. Crommie, C. P. Lutz, and D. M. Eigler, *Nature* **369**, 464 (1994).

³G. Meyer, S. Zophel, and K. H. Rieder, *Phys. Rev. Lett.* **77**, 2113 (1996).

⁴K. H. Rieder and A. Baratoff, *Phys. Bl.* **52**, 14 (1995).

⁵Ding-sheng Wang, Ruqian Wu, and A. J. Freeman, *Phys. Rev. B* **47**, 14 932 (1993).

- ⁶G. C. Fletcher, Proc. Phys. Soc. **65**, 192 (1952).
- ⁷J. C. Slater and G. F. Koster, Phys. Rev. **94**, 1498 (1954).
- ⁸H. Takayama, K.-P. Bohnen, and P. Fulde, Phys. Rev. B **14**, 2287 (1976).
- ⁹The angle θ denotes the angle between the magnetization direction z_M and the molecule axis or surface normal \hat{z} . ϕ is the angle between the x axis, and the projection of z_M in the plane of perpendicular magnetization or in the plane of the monolayer.
- ¹⁰P. N. Argyres, Phys. Rev. **97**, 334 (1955).
- ¹¹Of course, SOC *itself* is part of a perturbation expansion to the Dirac equation yielding the Pauli equation.
- ¹²M. Weinert, R. E. Watson, and J. W. Davenport, Phys. Rev. B **32**, 2115 (1990).
- ¹³Ding-shen Wang, Ruqian Wu, and A. J. Freeman, Phys. Rev. B **47**, 14 932 (1993); Phys. Rev. Lett. **70**, 869 (1993); **71**, 2166 (1993).
- ¹⁴G. H. O. Daalderop, P. J. Kelly, and M. R. H. Schuurmans, Phys. Rev. Lett. **71**, 2165 (1993).
- ¹⁵L. Szunyogh, B. Újfalussy, and P. Weinberger, Phys. Rev. B **51**, 9552 (1995).
- ¹⁶T. H. Moos, W. Hübner, and K. H. Bennemann, Solid State Commun. **98**, 639 (1996); T. H. Moos, Master's thesis, Freie Universität Berlin, 1995.
- ¹⁷It is well known that the 1D Ising-model, which is applicable for QW's and QR's (with periodic boundary conditions), exhibits a phase transition only at $T=0$. However, in our case we may implicitly assume hybridization with the substrate, which introduces some 2D character to our system.
- ¹⁸The 2D Heisenberg model should exhibit no phase transition if no anisotropy is involved; the latter, however, is the subject of this work. Thus the assumption of magnetic long-range order seems justified.
- ¹⁹S. E. Apsel, J. Deng, and L. A. Bloomfield, Phys. Rev. Lett. **76**, 1441 (1996).
- ²⁰Furthermore, Monte Carlo simulations for ferrofluids, where the only stable states for systems with few particles ($N < 14$) are the ring and the chain, show that rings always have an absolute magnetic moment that is close to zero for both low and high temperatures and nonzero magnetic field [indicating a radial moment configuration such as (i) and (h)]. Borrmann, Stamerjohanns, and Hilf (Ref. 21) expect that their results can also be transferred to nanocrystalline material.
- ²¹P. Borrmann, H. Stamerjohanns, and E. Hilf (unpublished).
- ²²J. Fassbender, U. May, B. Schirmer, R.M. Jungblut, B. Hillenbrands, and G. Güntherodt, Phys. Rev. Lett. **75**, 4476 (1995).
- ²³W. Weber, C. H. Back, Ch. Würsch, A. Bischof, and R. Allenspach, Phys. Rev. Lett. **76**, 1940 (1996).
- ²⁴This justifies using the same $n_d^{\text{eff}}=6.6$ as introduced for monolayers by Moos, Ref. 16.
- ²⁵M. Albrecht, T. Furubayashi, M. Przybylski, J. Korecki, and U. Gradmann, J. Magn. Mater. **113**, 207 (1992).
- ²⁶M. L. Néel, J. Phys. Rad. **15**, 225 (1954).
- ²⁷M. L. Néel, Comput. Rend. **237**, 1468 (1953).